GaSb-Based p-i-n Photodiodes With Partially Depleted Absorbers for High-Speed and High-Power Performance at 2.5-μm Wavelength

Jhih-Min Wun, Yu-Wen Wang, Yi-Han Chen, John E. Bowers, *Fellow, IEEE*, and Jin-Wei Shi, *Senior Member, IEEE*

***Abstract*— We first demonstrate a novel high-speed and high-power p-i-n photodiode with a cutoff wavelength at ∼2.5 μm. This device is composed of a partially depleted p-type $Ga_{0.8}In_{0.2}As_{0.16}Sb_{0.84}$ photo-absorption layer grown on GaSb substrate in order to enhance its speed and saturation power performance. With proper passivation processes, a low dark current (∼0.7 μA) and wide (6 GHz) optical-to-electrical (O-E) bandwidth can be simultaneously achieved with a miniaturized size of active mesa diameter (∼8 μm) under 1.55-μm optical wavelength excitation. The electron/hole drift-velocity and electron mobility across the $Ga_{0.8}In_{0.2}As_{0.16}Sb_{0.84}$ active layer can further be estimated based on the extracted internal response time and device modeling technique. Using the heterodyne-beating setup at 1.55-μm wavelength, the demonstrated device shows a saturation current at ∼3.6 mA (at 6-GHz operating frequency), which is mainly limited by the space-charge (electron/hole) induced screening effect at the depleted absorption region.**

***Index Terms*— Mid-infrared photonics, photodiodes.**

I. Introduction

HIGH-SPEED photodiodes that operate around the 2-μm wavelength are important for applications in mid-infrared (2–5 μm) Si photonics [1], environmental monitoring of greenhouses gases, high-resolution active light detection and ranging (LIDAR) sensors [2], and the photo-receivers in new generation optical fiber communication systems [3], [4]. The characteristic short response time of high-speed PDs can greatly enhance the resolution of a LIDAR system [2]. The high-speed performance and the maximum output saturation current are important figures-of-merit to ensuring a wide bandwidth and a large dynamic range. A high-power/speed PD, in conjunction with high-gain optical amplifier, such as thulium doped fiber amplifiers [4], can enhance the RF link gain in an analog system while also giving strong potential to produce excellent sensitivity in digital systems [5]. In this paper, we demonstrate a novel GaSb-based p-i-n photodiode, which has a cutoff wavelength at ∼2.5 μm and a partially depleted p-type $Ga_{0.8}In_{0.2}As_{0.16}Sb_{0.84}$ absorption layer in order to simultaneously achieve high-speed and high-power performance [6]–[8].

Compared with the reported InP-based PDs [2], [4] with a cutoff wavelength at around 2 μm, our proposed lattice-matched device structure is grown on an n-type GaSb substrate. The thick fully relaxed $InAs_xP_{1-x}$ [2] or $In_xGa_{1-x}As$ [4] buffer layers grown on the InP substrate can be totally eliminated. The quality of these buffer layers, which contain a lot of threading dislocation defects, is critical to the speed, dark current, and reliability performance of these InP-based 2-μm PDs [2], [4]. Furthermore, the detection wavelength window of the GaSb-based PD with a thick lattice-matched $Ga_xIn_{1-x}As_ySb_{1-y}$ alloy as the photo-absorption layer can be further extended to as long as ∼4 μm [9], which covers most of the midinfrared wavelengths (2–5 μm). Here, the dynamic high-speed and high output power performance obtained for this GaSb PD using the proposed device structure is first reported. Taking advantage of the characteristic of the strong photo-absorption process (∼1.5 μm^{-1}) in the $Ga_{0.8}In_{0.2}As_{0.16}Sb_{0.84}$ absorption layer under 1.55-μm wavelength excitation we perform device modeling/simulation on our PD, to extract the average electron/hole drift-velocity across the bulk $Ga_{0.8}In_{0.2}As_{0.16}Sb_{0.84}$ absorption layer.

II. Device Structure and Fabrication

Fig. 1(a) is a top-view of the fabricated device. Its epi-layer structure is described in Table I. Here, we adopted the structure of a typical vertical-illuminated photodiode with an active circular mesa and a p-type contact on the top. The diameter of the mesa is 8 μm. The whole epi-layer

Manuscript received March 14, 2016; revised April 22, 2016; accepted April 27, 2016. This work was supported by the Ministry Science and Technology, Taiwan, under Grant 102-2221-E-008-092-MY3. The review of this paper was arranged by Editor C. Surya.

J.-M. Wun, Y.-W. Wang, and Y.-H. Chen are with the Department of Electrical Engineering, National Central University, Taoyuan 320, Taiwan (e-mail: p3984011@hotmail.com; a072222685@yahoo.com.tw; willy111333@yahoo.com.tw).

J. E. Bowers is with the Department of Electrical and Computer Engineering, University of California at Santa Barbara, Santa Barbara, CA 93106 USA (e-mail: bowers@ece.ucsb.edu).

J.-W. Shi is with the University of California at Santa Barbara, Santa Barbara, CA 93106 USA, on leave from the National Central University, Taoyuan 320, Taiwan (e-mail: jwshi@ee.ncu.edu.tw; jwshi@ece.ucsb.edu).

Color versions of one or more of the figures in this paper are available online at http://ieeexplore.ieee.org.

Digital Object Identifier 10.1109/TED.2016.2561202

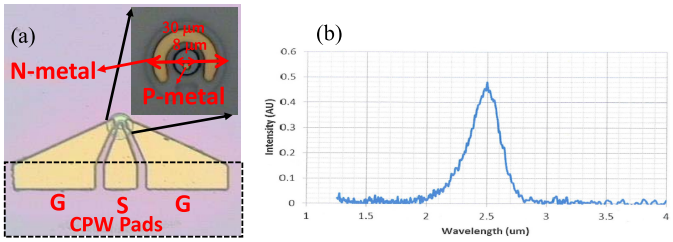

Fig. 1. (a) Top-view of demonstrated device: G: ground and S: signal. The area, where is surrounded by dashed line, represents the CPW pad. (b) Measured PL spectrum of epitaxial wafer used for device fabrication.

TABLE I
EPILAYER STRUCTURES

Layer	Material	Thickness (Å)	Doping Level (cm^{-3}) / Type	
P-Contact layer	GaSb	100	>1.0× 10^{19}	P+
Diffusion Block layer	$Al_{0.5}Ga_{0.5}Sb$	100	1.0 × 10^{19}	P+
Absorption layer I	GaSb	300	1.0 × 10^{19}	P+
Absorption layer II	$Ga_{0.8}In_{0.2}As_{0.16}Sb_{0.84}$	4000	5.0(bottom)-500(top)×10^{17}	P (graded)
Collector layer I	$Ga_{0.8}In_{0.2}As_{0.16}Sb_{0.84}$	4000	1.0 × 10^{16}	N-
Charge layer	$Ga_{0.8}In_{0.2}As_{0.16}Sb_{0.84}$	100	6.0 × 10^{16}	N
Collector layer II	$Ga_{0.8}In_{0.2}As_{0.16}Sb_{0.84}$	2900	1.0 × 10^{16}	N-
N Contact layer	GaSb	7000	8.0 × 10^{17}	N
Buffer Layer	GaSb	2000		i
Substrate	High resistivity GaSb substrate			

structure is grown on a 3-inch n-type GaSb substrate with a doping density in the range of 3.8×10^{16} to 7.1×10^{16} cm^{-3}. From top to bottom, it is composed of a 10 nm p^+ GaSb (Be doped: 1×10^{19} cm^{-3}) ohmic contact layer, a 10 nm $Al_{0.5}Ga_{0.5}Sb$ p^+ (1×10^{19} cm^{-3}) diffusion blocking layer, a 1.1 μm $Ga_{0.8}In_{0.2}As_{0.16}Sb_{0.84}$ photo-absorption layer, and a 700 nm N-type (Te doped: 8×10^{17} cm^{-3}) GaSb contact layer. The photoluminescence (PL) measurement results for our device structure, given in Fig. 1(b), showing the PL peak at a wavelength of 2.5 μm wavelength.

This indicates that the absorption edge of our proposed PD structure should be located around this wavelength. In the thick (1.1 μm) $Ga_{0.8}In_{0.2}As_{0.16}Sb_{0.84}$ photo-absorption layer, there is a 400-nm p-type undepleted layer with a graded doping profile [5×10^{19} cm^{-3} (top) to 5×10^{17} cm^{-3} (bottom)]. The partially depleted p-type layer with the graded doping profile inside the absorption region can minimize the transit time of holes and has been demonstrated to further enhance the saturation output power performance in $InP/In_{0.53}Ga_{0.47}As$ photodiodes [10], [11]. The residual 700-nm absorption layer in our structure is left for n^- doping (1×10^{16} cm^{-3}). In such an n^- region, there is an additional 10-nm n-type charge layer (6×10^{16} cm^{-3}) near the cathode. The purpose of this charge layer is to allow the externally applied electric field to be more concentrated near the p-/n-junction in the absorption region, which can effectively minimize the space-charge screening effect under the desired reverse bias voltage [12]. The fabrication of our device includes mesa etching to the GaSb n-type contact layer after which deposition/annealing of the p (Ti/Au)- and n (Ni/Ge/Au)-contact metal is performed. After the second run of mesa etching to

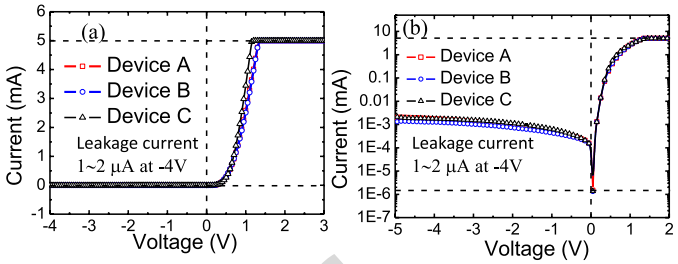

Fig. 2. Measured dark I–V curves of devices with (a) linear and (b) long-scale.

the n-type GaSb substrate, the device is carefully passivated by the growth of a SiO_2 film near room temperature so as to avoid surface damage. As shown in Fig. 1(a), for the purpose of on-wafer measurement, the fabricated device is integrated with a coplanar waveguide (CPW) pad on the GaSb substrate, with a SiO_2 film deposited on top of it to avoid leakage current from the n-type GaSb substrate.

III. MEASUREMENT RESULTS

Fig. 2(a) and (b) shows three typical current (I)–voltage (V) curves for the fabricated devices across different parts and wafers given in linear and log-scale, respectively. As can be seen, our device can have significant rectifying behavior with a low dark current under a high reverse bias voltage. Under forward bias operation with a turn-ON voltage at ~0.5 V, the measured differential resistance is around 140 Ω, mainly due to the contact and bulk resistance of the n-type GaSb layers. A smaller value of n-contact resistance can be expected by further increasing the n-type (Te) doping density (8×10^{17} cm^{-3}) in our contact layer. However, such an approach would induce significant out-diffusion of the tellurium dopant during material growth and have a serious influence on device performance [13].

In order to attain very high-speed PD performance, a miniaturized size of device active diameter (<10 μm) is necessary in order to relax the RC-limited bandwidth. However, this usually leads to a significant increase of the leakage current contributed from the surface state. However, thanks to our device passivation process, the measured dark current of our device with a miniaturized active diameter (8 μm) is as small as 0.7–1 μA under −2 V bias, which is the typical operational bias voltage for high-speed performance of the device under low output photocurrent operation. In addition, for high output power from a PD, a further increase in the reverse bias voltage is definitely necessary to overcome the space-charge screening effect. As can be seen, the dark current is still low (1–2 μA) when the reverse bias reaches −5 V. The reported dark current values here are close to those of the state-of-the-art InP-based 2-μm wavelength PDs (several μAs) [3]. Such results imply that good surface passivation has been achieved with our device.

Under 1.55-μm wavelength excitation and −2 V bias, the measured dc responsivity is around 0.4 A/W, which corresponds to 32% external quantum efficiency. Due to the strong photo-absorption process in the $Ga_{0.8}In_{0.2}As_{0.16}Sb_{0.84}$ layer

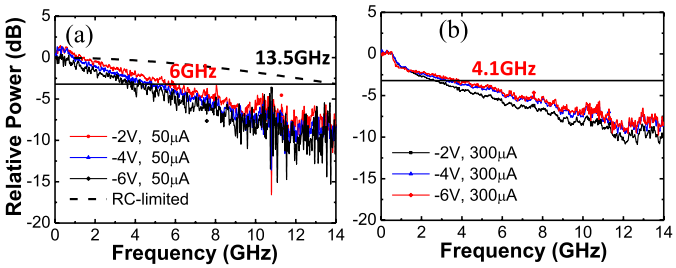

Fig. 3. Measured bias-dependent O-E frequency responses of devices under (a) low (0.05 mA) and (b) high (0.3 mA) output photocurrents.

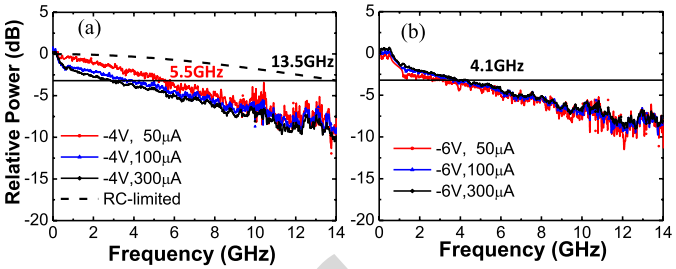

Fig. 4. Measured O-E frequency responses of devices under different output photocurrents and two reverse bias voltage at (a) −4 and (b) −6 V.

under 1.55-μm wavelength excitation [14], we can expect most of the photo-generated carrier to be concentrated in the topmost p-/n-junction and the contribution from the GaSb substrate can be neglected. Considering the optical reflection loss, there remains around 57% of the photo-generated carrier to be recombined inside the p-type absorber. This number is much larger than that of the InP-based PDs, showing a nearly negligible recombination loss in the p-type $In_{0.53}G_{0.47}$aAs-based absorber layer and excellent efficiency performance, even under short-wavelength (0.85 μm) excitation with a huge absorption process ($\sim$3 μm^{-1}) [15], [16]. This result indicates a much higher defect density and smaller mobility of photo-generated carriers in our GaSb-based material system than that of InP-based ones. The measured defect mapping results of the topmost layer of our wafer structure show a defect density over ten times larger than what is typical of the InP-based PD epitaxy wafers.

Fig. 3(a) and (b) shows the bias-dependent optical-to-electrical (O-E) frequency responses measured under low (0.05 mA) and high (0.3 mA) output photocurrents, respectively. The dotted line in Fig. 3(a) represents the extracted *RC*-limited frequency response of our device, which will be discussed in detail later. As can be seen, under a low output photocurrent (0.05 mA), the widest 3-dB O-E bandwidth is around 6 GHz under −2 V bias and a further increase in the reverse bias voltage (to −4 and −6 V) would lead to a slight degradation in the speed performance. This phenomenon will be discussed later in relation to the measured optical power dependent O-E frequency response, as shown in Fig. 4. On the other hand, when the output photocurrent reaches 0.3 mA, a higher reverse (−4 V) bias voltage is necessary to compensate for the space-charge screening effect induced bandwidth degradation, which is similar to the typical dynamic behavior of high-speed p-i-n PDs [17].

Fig. 4(a) and (b) shows the O-E frequency responses measured under different output photocurrents and two fixed reverse bias voltages −4 and −6 V, respectively. We can clearly see that under a −4 V bias voltage, the O-E bandwidth degrades with the increase in output photocurrent (0.05 to 0.3 mA) as expected, and a high reverse bias (−6 V) can minimize such phenomenon of speed degradation. Under a small output photocurrent (0.05 mA), a high reverse bias (−6 V) degrades the 3-dB O-E bandwidth (5.5–4 GHz). This result can be observed in Fig. 3(a) and can be attributed to the intervalley scattering effect of photo-generated electrons in the $Ga_{0.8}In_{0.2}As_{0.16}Sb_{0.84}$ absorption layer becoming more significant with the increase in reverse bias. This thus leads to a degradation of the internal transit time-limited bandwidth. On the other hand, under a high output photocurrent, the electron/hole induced space-charge screening effect saturates the output of the PD and also diminishes the intervalley scattering effect of the electrons. Similar dynamic behavior has been reported in InP/$In_{0.53}Ga_{0.47}$As-based PDs under short-wavelength (850 nm) excitation. Compared with the case being studied here, the observed O-E bandwidth degradation under high reverse bias voltage is more significant in the InP/$In_{0.53}Ga_{0.47}$As-based PDs due to the fact that a p-type $In_{0.53}Ga_{0.47}$As absorber has a much larger absorption constant ($\sim$3 versus $\sim$1.5 μm^{-1}) than that of a $Ga_{0.8}In_{0.2}As_{0.16}Sb_{0.84}$ absorption layer under 0.85 and 1.55 μm wavelength excitation, respectively [14]–[16]. A stronger photo-absorption process in the p-type absorber represents a smaller number of photo-generated holes drifting in the intrinsic region and the electrons play a more important role in the dynamic behavior of the PDs.

As shown in Fig. 3(a), the extracted *RC*-limited frequency response can be as high as 13.5 GHz, which implies that the net O-E bandwidth is mainly dominated by the internal carrier transit time. Here, the equivalent circuit modeling technique was performed to extract these parameters for our device [12], [15], [16].

The overall O-E 3-dB bandwidth (f_{3dB}) of a PD is determined by the carrier transport time ($1/f_t$) and the *RC* time constant ($1/f_{RC}$). In order to investigate the internal carrier transport time inside our device, the following equation is adopted [16]:

$$\frac{1}{f_{3dB}^2} = \frac{1}{f_{RC}^2} + \frac{1}{f_t^2} = (2\pi RC)^2 + \frac{1}{f_t^2} \quad (1)$$

where R is the sum of the parasitic resistance and the load resistance (50 Ω) and C is the total capacitance. Here, the *RC*-limited bandwidth can be extracted by the use of the measured scattering parameters of the microwave reflection coefficients (S_{11}) [12], [15], [16]. Fig. 5(a) shows the adopted equivalent circuit models for the fitting of the S_{11} parameters and the fitted values of each circuit element, except for R_T and C_T, are shown in the table inserted into Fig. 5(b). During the device modeling process for the extraction of the extrinsic f_{RC} for the PD chips, two artificial circuit elements (R_T and C_T) are removed due to the fact that they are

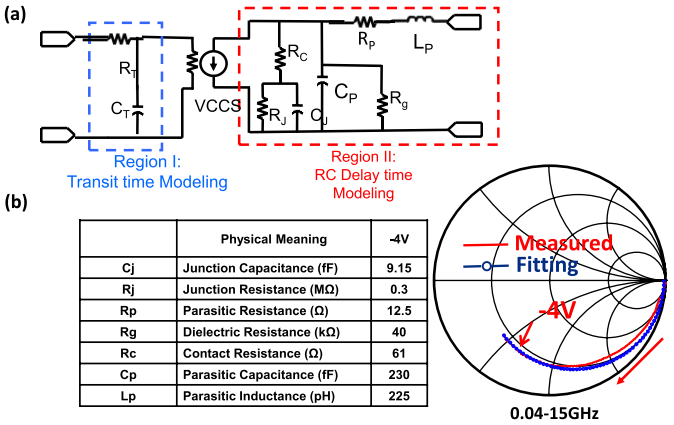

	Physical Meaning	-4V
Cj	Junction Capacitance (fF)	9.15
Rj	Junction Resistance (MΩ)	0.3
Rp	Parasitic Resistance (Ω)	12.5
Rg	Dielectric Resistance (kΩ)	40
Rc	Contact Resistance (Ω)	61
Cp	Parasitic Capacitance (fF)	230
Lp	Parasitic Inductance (pH)	225

Fig. 5. (a) Adopted equivalent circuit model for device modeling. (b) Measured and fitted S_{11} parameters (microwave reflection coefficient) of the device on Smith chart. The arrow head represents the increasing of sweeping frequency. The inserted table shows the values of circuit elements used for the modeling process (voltage-controlled current source).

used to mimic the low-pass frequency response of the internal carrier transit time [12], [15], [16]. Fig. 5(b) shows the fitted and measured S_{11} parameters in the Smith chart while the extracted *RC*-limited frequency responses are given in Figs. 3(a) and 4(a), as discussed above. We can clearly see that the fitted trace matches well with the measured ones from nearly dc to 15 GHz. By use of the extracted *RC*-limited frequency response and (1), the extracted internal carrier transit time-limited bandwidth under 1.55-μm wavelength excitation and 0.05 mA output photocurrent is around 6.7 GHz.

In order to further understand the mechanism behind such a small transit time-limited bandwidth, we simulated the internal frequency responses of our device under 1.55-μm wavelength excitations. The simulation results should let us know the estimated electron/hole drift-velocities and minority diffusion coefficients across intrinsic and p-type $Ga_{0.8}In_{0.2}As_{0.16}Sb_{0.84}$ absorbers, respectively. The adopted drift-diffusion model for bandwidth calculation can be found in [18] and the parameters used for simulation are given in Table II. Here, we assume that our $Ga_{0.8}In_{0.2}As_{0.16}Sb_{0.84}$ absorption layer has a photo-absorption constant as large as 1.5 μm^{-1}, which is close to that of InAs ($\sim$2.0 μm^{-1}) under the same wavelength excitation [19]. These absorption constant values suggest that around 60% of the photo-generated carriers will be concentrated in the topmost 0.6-μm absorption region ($\approx e^{-1}$). The fitted electron/hole drift-velocities and minority (electron) diffusion coefficients in the p-type absorber for the around 7-GHz transit bandwidth are much smaller than the numbers typical in the InP/InGaAs material systems. Take the fitted value of the electron diffusion coefficient ($\sim$200 $cm^2/V \cdot s$) for example. It is over 20 times smaller than that of in the p-type $In_{0.53}Ga_{0.47}As$ absorber ($\sim$5000 $cm^2/V \cdot s$) [17]. This explains the significant recombination process in the p-type absorber and the degradation in the measured EQE value as discussed above.

Fig. 6 represents the photo-generated RF power measured at 6 GHz under three different bias voltages (-3, -4, and -6 V). The ideal relation between the RF power of a 100% modulated large-signal and the average current for

TABLE II
SIMULATION PARAMETERS

	Wavelength:1550 nm
Optical Absorption Constant of $Ga_{0.8}In_{0.2}As_{0.16}Sb_{0.84}$	1.5 μm^{-1}
Effective Absorption Depth (e^{-1})	0.6 μm
Minority Electron Mobility in graded p-doped $Ga_{0.8}In_{0.2}As_{0.16}Sb_{0.84}$	200 cm^2/V-sec
Electron Drift-Velocity in Intrinsic $Ga_{0.8}In_{0.2}As_{0.16}Sb_{0.84}$	2×10^4 m/sec
Hole Drift-Velocity in Intrinsic $Ga_{0.8}In_{0.2}As_{0.16}Sb_{0.84}$	1×10^4 m/sec
Effective Electron Drift Distance at $Ga_{0.8}In_{0.2}As_{0.16}Sb_{0.84}$ Layer	0.5 μm
Effective Hole Drift Distance at $Ga_{0.8}In_{0.2}As_{0.16}Sb_{0.84}$ Layer	0.2 μm

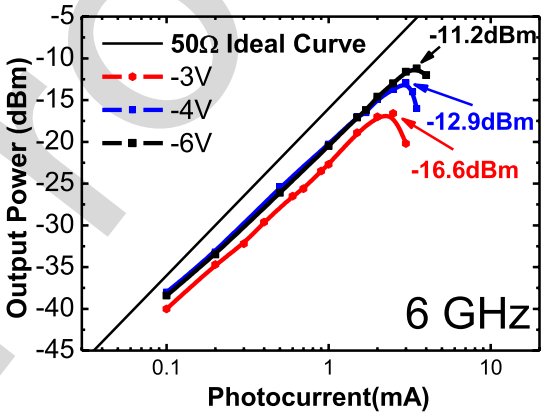

Fig. 6. Measured photo-generated RF power versus photocurrent of demonstrated PD under sinusoidal signal excitations and different reverse biases at an operating frequency of 6 GHz. Solid line: the ideal trace for a 100% modulation depth and 50-Ω load.

a 50 Ω (straight line) load is also plotted for reference. As can be seen, the maximum output saturation current is proportional to the increase in reverse bias voltage. Under -6 V bias, the highest saturation current is limited to around 3.6 mA. In addition, there is an approximately 3–5 dB difference between the measured and ideal RF power under different output photocurrents. Such a discrepancy is mainly due to the high-frequency roll-off in the O-E frequency response of the device itself. As shown in Fig. 3(b), the high-frequency roll-off at 6 GHz in the measured trace under an output photocurrent of 0.3 mA and -6 V reverse bias is around 4 dB, which is consistent with the photo-generated RF power measurement results, as discussed here.

According to our static electric (E) field simulation, the E-field around the p-type absorber and n-type charge layer is around 100 kV/cm under -6 V bias. Use the fitted hole velocities listed in Table II and following (2) [17], the space-charge (hole) induced field under near saturation output ($\sim$3.6 mA) is around $\sim$100 kV/cm. This value is close to the external applied E-field under -6 V bias, which implies that our extracted values for the carrier drift-velocities are

reasonable and consistent with our measurement results. In this equation, E_{sc} represents the space-charge induced field, ε is the dielectric constant of the $Ga_{0.8}In_{0.2}As_{0.16}Sb_{0.84}$ absorption layer, which is around 15 ε_0 [14], and V_c is effective carrier (hole) drift-velocity (1×100^4 m/s). Here, the depletion layer thickness D_{dep} is assumed to be $\sim$0.2 μm. This number is determined by the effective absorption depth (e^{-1}; $\sim$0.6 μm) and the thickness of the p-type absorber ($\sim$0.4 μm) layer in the device structure

$$E_{sc} = J_{max}\left(\frac{D_{dep}}{\varepsilon V_c}\right). \quad (2)$$

The results indicate that the saturation power in our device is limited by the small carrier drift-velocity and its induced space-charge screening effect.

IV. Conclusion

A high-speed and high-power GaSb-based PD with a cutoff wavelength at around 2.5 μm was demonstrated for the first time. The addition of a partially depleted absorber layer has been implemented in our structure to minimize the space-charge screening effect and improve the high-power/speed performance. Furthermore, a miniaturized device size (active diameter: 8 μm) is adopted to enlarge the *RC*-limited bandwidth. With careful passivation to minimize the influence of the surface state, low dark current can still be sustained ($\sim$0.7 μA at -2 V) in such a small device. According to the measurement and modeling results under 1.55-μm optical wavelength excitation, the slow carrier drift/diffusion time inside our $Ga_{0.8}In_{0.2}As_{0.16}Sb_{0.84}$ active layers is the major factor limiting the speed and output power. A 3.6-mA saturation current measured at the 6-GHz operating frequency can be achieved. The PD demonstrates good speed and power performance at a wavelength of 2.5 μm so should find applications in midinfrared (2–5 μm) Si photonics, high-resolution/frame rate LIDAR image sensors, and photo-receivers in next-generation optical fiber communication channels.

References

[1] R. Soref, "Mid-infrared photonics in silicon and germanium," *Nature Photon.*, vol. 4, pp. 495–497, Aug. 2010.

[2] A. Joshi and S. Datta, "High-speed, large-area, p-i-n InGaAs photodiode linear array at 2-micron wavelength," *Proc. SPIE*, vol. 8353, p. 83533D, May 2012.

[3] J. E. Bowers, A. K. Srivastava, C. A. Burrus, M. A. DeWinter, M. A. Pollack, and J. L. Zyskind, "High-speed GaInAsSb/GaSb PIN photodetectors for wavelengths to 2.3 μm," *Electron. Lett.*, vol. 22, pp. 137–138, Jan. 1986.

[4] N. Ye *et al.*, "InGaAs surface normal photodiode for 2 μm optical communication systems," *IEEE Photon. Technol. Lett.*, vol. 27, no. 14, pp. 1469–1472, Jul. 15, 2015.

[5] Y. Miyamoto, M. Yoneyama, K. Hagimoto, T. Ishibashi, and N. Shimizu, "40 Gbit/s high sensitivity optical receiver with uni-travelling-carrier photodiode acting as decision IC driver," *Electron. Lett.*, vol. 34, no. 2, pp. 214–215, Jan. 1998.

[6] X. Li *et al.*, "High-saturation-current InP-InGaAs photodiode with partially depleted absorber," *IEEE Photon. Technol. Lett.*, vol. 15, no. 9, pp. 1276–1278, Sep. 2003.

[7] Y. Muramoto and T. Ishibashi, "InP/InGaAs pin photodiode structure maximising bandwidth and efficiency," *Electron. Lett.*, vol. 39, no. 24, pp. 1749–1750, Nov. 2003.

[8] I. A. Andreev *et al.*, "High-speed photodiodes for the mid-infrared spectral region 1.2–2.4 μm based on GaSb/GaInAsSb/GaAlAsSb heterostructures with a transmission band of 2–5 GHz," *Semiconductors*, vol. 47, no. 8, pp. 1103–1109, Aug., 2013.

[9] A. Rakovska *et al.*, "Room temperature InAsSb photovoltaic midinfrared detector," *Appl. Phys. Lett.*, vol. 77, no. 3, pp. 397–399, Jul. 2000.

[10] X. Li *et al.*, "A partially depleted absorber photodiode with graded doping injection regions," *IEEE Photon. Technol. Lett.*, vol. 16, no. 10, pp. 2326–2328, Oct. 2004.

[11] Y.-S. Wu *et al.*, "High-performance evanescently edge coupled photodiodes with partially p-doped photoabsorption layer at 1.55-μm wavelength," *IEEE Photon. Technol. Lett*, vol. 17, no. 4, pp. 878–880, Apr. 2005.

[12] J.-M. Wun *et al.*, "Photonic high-power continuous wave THz-wave generation by using flip-chip packaged uni-traveling carrier photodiodes and a femtosecond optical pulse generator," *J. Lightw. Technol.*, vol. 34, no. 4, pp. 1387–1397, Feb. 15, 2016.

[13] T. I. Voronina *et al.*, "The effect of tellurium diffusion from an *n*-GaSb:Te substrate on the properties of GaInAsSb solid solutions grown from lead-containing melt," *Semiconductors*, vol. 39, pp. 308–312, Mar. 2005.

[14] M. P. Mikhailova, *Handbook Series on Semiconductor Parameters*, vol. 2, M. Levinshtein, S. Rumyantsev, and M. Shur, Eds. London, U.K.: World Scientific, 1999, pp. 180–205.

[15] J.-W. Shi, C.-Y. Li, K.-L. Chi, J.-M. Wun, Y.-M. Hsin, and S. D. Benjamin, "Large-area p-i-n photodiode with high-speed and high-efficiency across a wide optical operation window (0.85 to 1.55 μm)," *IEEE J. Sel. Topics Quantum Electron.*, vol. 20, no. 6, Nov./Dec. 2014, Art. no. 3800807.

[16] J.-W. Shi, K.-L. Chi, C.-Y. Li, and J.-M. Wun, " Dynamic analysis of high-efficiency InP-based photodiode for 40 Gbit/s optical interconnect across a wide optical window (0.85 to 1.55 μm)," *J. Lightw. Technol.*, vol. 33, no. 4, pp. 921–927, Feb. 15, 2015.

[17] K. Kato, "Ultrawide-band/high-frequency photodetectors," *IEEE Trans. Microw. Theory Techn.*, vol. 47, no. 7, pp. 1265–1281, Jul. 1999.

[18] J.-W. Shi, Y.-H. Liu, and C.-W. Liu, "Design and analysis of separate-absorption-transport-charge-multiplication traveling-wave avalanche photodetectors," *J. Lightw. Technol.*, vol. 22, no. 6, pp. 1583–1590, Jun. 2004.

[19] M. P. Mikhailova, *Handbook Series on Semiconductor Parameters*, vol. 1, M. Levinshtein, S. Rumyantsev, and M. Shur, Eds. London, U.K.: World Scientific, 1996, pp. 147–168.

Jhih-Min Wun was born in Taoyuan, Taiwan, in 1988. He is currently pursuing the Ph.D. degree with the Department of Electrical Engineering, National Central University, Taoyuan.

His current research interests include high-speed optoelectronic device measurement and sub-THz high-speed photodiode.

Yu-Wen Wang was born in Kaohsiung, Taiwan, in 1992. He is currently pursuing the master's degree with the Department of Electrical Engineering, National Central University, Taoyuan, Taiwan.

His current research interests include high-speed and high-power photodiode.

Yi-Han Chen was born in Kaohsiung, Taiwan, in 1992. He is currently pursuing the master's degree with the Department of Electrical Engineering, National Central University, Taoyuan, Taiwan.

His current research interests include high-speed and high-sensitivity avalanche photodiode.

John E. Bowers (F'93) holds the Fred Kavli Chair in Nanotechnology, and is the Director of the Institute for Energy Efficiency and a Professor with the Department of Materials and Electrical and Computer Engineering, University of California at Santa Barbara, Santa Barbara, CA, USA. He is a Co-Founder of Aurrion, Santa Barbara, CA, Aerius Photonics, Ventura, CA, USA, and Calient Networks, Goleta, CA, USA.

Jin-Wei Shi (M'03–SM'12) was born in Kaohsiung, Taiwan in 1976.

He joined the Department of Electrical Engineering, National Central University, Taoyuan, Taiwan, in 2003, where he has been a professor since 2011. He joined the Department of Materials and Electrical and Computer Engineering, University of California at Santa Barbara, Santa Barbara, CA, USA, as a Visiting Professor, in 2011 and 2012 and 2016. He has authored or co-authored over four book chapters, 120 journal papers, 180 conference papers, and hold 30 patents. His current research interests include ultra-high speed/power photodetectors, electro-absorption modulator, THz photonic transmitter, and VCSELs.

Dr. Shi was a recipient of 2010 Da-You Wu Memorial Award.

GaSb-Based p-i-n Photodiodes With Partially Depleted Absorbers for High-Speed and High-Power Performance at 2.5-μm Wavelength

Jhih-Min Wun, Yu-Wen Wang, Yi-Han Chen, John E. Bowers, *Fellow, IEEE*, and Jin-Wei Shi, *Senior Member, IEEE*

***Abstract*— We first demonstrate a novel high-speed and high-power p-i-n photodiode with a cutoff wavelength at ∼2.5 μm. This device is composed of a partially depleted p-type $Ga_{0.8}In_{0.2}As_{0.16}Sb_{0.84}$ photo-absorption layer grown on GaSb substrate in order to enhance its speed and saturation power performance. With proper passivation processes, a low dark current (∼0.7 μA) and wide (6 GHz) optical-to-electrical (O-E) bandwidth can be simultaneously achieved with a miniaturized size of active mesa diameter (∼8 μm) under 1.55-μm optical wavelength excitation. The electron/hole drift-velocity and electron mobility across the $Ga_{0.8}In_{0.2}As_{0.16}Sb_{0.84}$ active layer can further be estimated based on the extracted internal response time and device modeling technique. Using the heterodyne-beating setup at 1.55-μm wavelength, the demonstrated device shows a saturation current at ∼3.6 mA (at 6-GHz operating frequency), which is mainly limited by the space-charge (electron/hole) induced screening effect at the depleted absorption region.**

***Index Terms*— Mid-infrared photonics, photodiodes.**

I. Introduction

HIGH-SPEED photodiodes that operate around the 2-μm wavelength are important for applications in mid-infrared (2–5 μm) Si photonics [1], environmental monitoring of greenhouses gases, high-resolution active light detection and ranging (LIDAR) sensors [2], and the photo-receivers in new generation optical fiber communication systems [3], [4]. The characteristic short response time of high-speed PDs can greatly enhance the resolution of a LIDAR system [2]. The high-speed performance and the maximum output saturation current are important figures-of-merit to ensuring a wide bandwidth and a large dynamic range. A high-power/speed PD, in conjunction with high-gain optical amplifier, such as thulium doped fiber amplifiers [4], can enhance the RF link gain in an analog system while also giving strong potential to produce excellent sensitivity in digital systems [5]. In this paper, we demonstrate a novel GaSb-based p-i-n photodiode, which has a cutoff wavelength at ∼2.5 μm and a partially depleted p-type $Ga_{0.8}In_{0.2}As_{0.16}Sb_{0.84}$ absorption layer in order to simultaneously achieve high-speed and high-power performance [6]–[8].

Compared with the reported InP-based PDs [2], [4] with a cutoff wavelength at around 2 μm, our proposed lattice-matched device structure is grown on an n-type GaSb substrate. The thick fully relaxed $InAs_xP_{1-x}$ [2] or $In_xGa_{1-x}As$ [4] buffer layers grown on the InP substrate can be totally eliminated. The quality of these buffer layers, which contain a lot of threading dislocation defects, is critical to the speed, dark current, and reliability performance of these InP-based 2-μm PDs [2], [4]. Furthermore, the detection wavelength window of the GaSb-based PD with a thick lattice-matched $Ga_xIn_{1-x}As_ySb_{1-y}$ alloy as the photo-absorption layer can be further extended to as long as ∼4 μm [9], which covers most of the midinfrared wavelengths (2–5 μm). Here, the dynamic high-speed and high output power performance obtained for this GaSb PD using the proposed device structure is first reported. Taking advantage of the characteristic of the strong photo-absorption process (∼1.5 μm^{-1}) in the $Ga_{0.8}In_{0.2}As_{0.16}Sb_{0.84}$ absorption layer under 1.55-μm wavelength excitation we perform device modeling/simulation on our PD, to extract the average electron/hole drift-velocity across the bulk $Ga_{0.8}In_{0.2}As_{0.16}Sb_{0.84}$ absorption layer.

II. Device Structure and Fabrication

Fig. 1(a) is a top-view of the fabricated device. Its epi-layer structure is described in Table I. Here, we adopted the structure of a typical vertical-illuminated photodiode with an active circular mesa and a p-type contact on the top. The diameter of the mesa is 8 μm. The whole epi-layer

Manuscript received March 14, 2016; revised April 22, 2016; accepted April 27, 2016. This work was supported by the Ministry Science and Technology, Taiwan, under Grant 102-2221-E-008-092-MY3. The review of this paper was arranged by Editor C. Surya.

J.-M. Wun, Y.-W. Wang, and Y.-H. Chen are with the Department of Electrical Engineering, National Central University, Taoyuan 320, Taiwan (e-mail: p3984011@hotmail.com; a072222685@yahoo.com.tw; willy111333@yahoo.com.tw).

J. E. Bowers is with the Department of Electrical and Computer Engineering, University of California at Santa Barbara, Santa Barbara, CA 93106 USA (e-mail: bowers@ece.ucsb.edu).

J.-W. Shi is with the University of California at Santa Barbara, Santa Barbara, CA 93106 USA, on leave from the National Central University, Taoyuan 320, Taiwan (e-mail: jwshi@ee.ncu.edu.tw; jwshi@ece.ucsb.edu).

Color versions of one or more of the figures in this paper are available online at http://ieeexplore.ieee.org.

Digital Object Identifier 10.1109/TED.2016.2561202

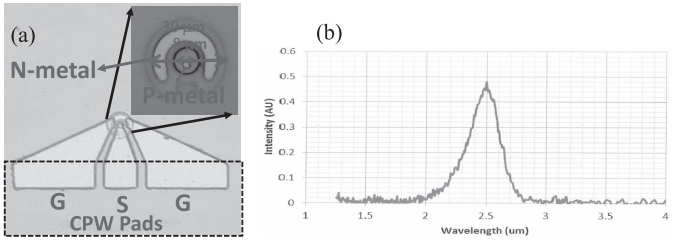

Fig. 1. (a) Top-view of demonstrated device: G: ground and S: signal. The area, where is surrounded by dashed line, represents the CPW pad. (b) Measured PL spectrum of epitaxial wafer used for device fabrication.

TABLE I
EPILAYER STRUCTURES

Layer	Material	Thickness (Å)	Doping Level (cm^{-3}) / Type	
P-Contact layer	GaSb	100	>1.0× 10^{19}	P+
Diffusion Block layer	$Al_{0.5}Ga_{0.5}Sb$	100	1.0 × 10^{19}	P+
Absorption layer I	GaSb	300	1.0 × 10^{19}	P+
Absorption layer II	$Ga_{0.8}In_{0.2}As_{0.16}Sb_{0.84}$	4000	5.0(bottom)-500(top)×10^{17}	P (graded)
Collector layer I	$Ga_{0.8}In_{0.2}As_{0.16}Sb_{0.84}$	4000	1.0 × 10^{16}	N-
Charge layer	$Ga_{0.8}In_{0.2}As_{0.16}Sb_{0.84}$	100	6.0 × 10^{16}	N
Collector layer II	$Ga_{0.8}In_{0.2}As_{0.16}Sb_{0.84}$	2900	1.0 × 10^{16}	N-
N Contact layer	GaSb	7000	8.0 × 10^{17}	N
Buffer Layer	GaSb	2000		i
Substrate	High resistivity GaSb substrate			

structure is grown on a 3-inch n-type GaSb substrate with a doping density in the range of 3.8×10^{16} to 7.1×10^{16} cm^{-3}. From top to bottom, it is composed of a 10 nm p^+ GaSb (Be doped: 1×10^{19} cm^{-3}) ohmic contact layer, a 10 nm $Al_{0.5}Ga_{0.5}Sb$ p^+ (1×10^{19} cm^{-3}) diffusion blocking layer, a 1.1 μm $Ga_{0.8}In_{0.2}As_{0.16}Sb_{0.84}$ photo-absorption layer, and a 700 nm N-type (Te doped: 8×10^{17} cm^{-3}) GaSb contact layer. The photoluminescence (PL) measurement results for our device structure, given in Fig. 1(b), showing the PL peak at a wavelength of 2.5 μm wavelength.

This indicates that the absorption edge of our proposed PD structure should be located around this wavelength. In the thick (1.1 μm) $Ga_{0.8}In_{0.2}As_{0.16}Sb_{0.84}$ photo-absorption layer, there is a 400-nm p-type undepleted layer with a graded doping profile [5×10^{19} cm^{-3} (top) to 5×10^{17} cm^{-3} (bottom)]. The partially depleted p-type layer with the graded doping profile inside the absorption region can minimize the transit time of holes and has been demonstrated to further enhance the saturation output power performance in $InP/In_{0.53}Ga_{0.47}As$ photodiodes [10], [11]. The residual 700-nm absorption layer in our structure is left for n^- doping (1×10^{16} cm^{-3}). In such an n^- region, there is an additional 10-nm n-type charge layer (6×10^{16} cm^{-3}) near the cathode. The purpose of this charge layer is to allow the externally applied electric field to be more concentrated near the p-/n-junction in the absorption region, which can effectively minimize the space-charge screening effect under the desired reverse bias voltage [12]. The fabrication of our device includes mesa etching to the GaSb n-type contact layer after which deposition/annealing of the p (Ti/Au)- and n (Ni/Ge/Au)-contact metal is performed. After the second run of mesa etching to

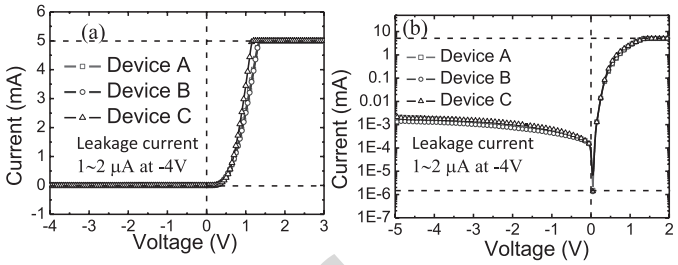

Fig. 2. Measured dark I–V curves of devices with (a) linear and (b) long-scale.

the n-type GaSb substrate, the device is carefully passivated by the growth of a SiO_2 film near room temperature so as to avoid surface damage. As shown in Fig. 1(a), for the purpose of on-wafer measurement, the fabricated device is integrated with a coplanar waveguide (CPW) pad on the GaSb substrate, with a SiO_2 film deposited on top of it to avoid leakage current from the n-type GaSb substrate.

III. MEASUREMENT RESULTS

Fig. 2(a) and (b) shows three typical current (I)–voltage (V) curves for the fabricated devices across different parts and wafers given in linear and log-scale, respectively. As can be seen, our device can have significant rectifying behavior with a low dark current under a high reverse bias voltage. Under forward bias operation with a turn-ON voltage at ∼0.5 V, the measured differential resistance is around 140 Ω, mainly due to the contact and bulk resistance of the n-type GaSb layers. A smaller value of n-contact resistance can be expected by further increasing the n-type (Te) doping density (8×10^{17} cm^{-3}) in our contact layer. However, such an approach would induce significant out-diffusion of the tellurium dopant during material growth and have a serious influence on device performance [13].

In order to attain very high-speed PD performance, a miniaturized size of device active diameter (<10 μm) is necessary in order to relax the *RC*-limited bandwidth. However, this usually leads to a significant increase of the leakage current contributed from the surface state. However, thanks to our device passivation process, the measured dark current of our device with a miniaturized active diameter (8 μm) is as small as 0.7–1 μA under −2 V bias, which is the typical operational bias voltage for high-speed performance of the device under low output photocurrent operation. In addition, for high output power from a PD, a further increase in the reverse bias voltage is definitely necessary to overcome the space-charge screening effect. As can be seen, the dark current is still low (1–2 μA) when the reverse bias reaches −5 V. The reported dark current values here are close to those of the state-of-the-art InP-based 2-μm wavelength PDs (several μAs) [3]. Such results imply that good surface passivation has been achieved with our device.

Under 1.55-μm wavelength excitation and −2 V bias, the measured dc responsivity is around 0.4 A/W, which corresponds to 32% external quantum efficiency. Due to the strong photo-absorption process in the $Ga_{0.8}In_{0.2}As_{0.16}Sb_{0.84}$ layer

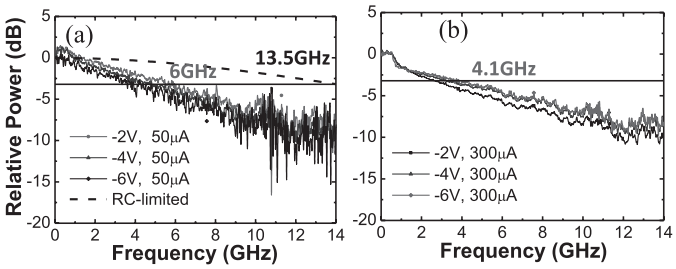

Fig. 3. Measured bias-dependent O-E frequency responses of devices under (a) low (0.05 mA) and (b) high (0.3 mA) output photocurrents.

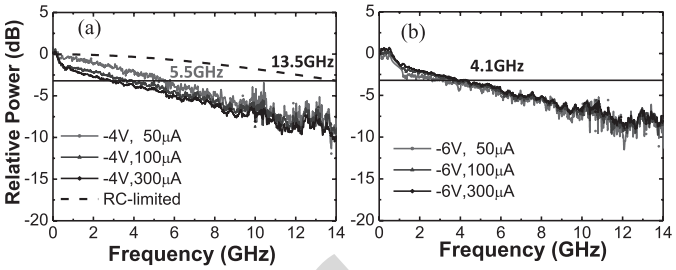

Fig. 4. Measured O-E frequency responses of devices under different output photocurrents and two reverse bias voltage at (a) −4 and (b) −6 V.

under 1.55-μm wavelength excitation [14], we can expect most of the photo-generated carrier to be concentrated in the topmost p-/n-junction and the contribution from the GaSb substrate can be neglected. Considering the optical reflection loss, there remains around 57% of the photo-generated carrier to be recombined inside the p-type absorber. This number is much larger than that of the InP-based PDs, showing a nearly negligible recombination loss in the p-type $In_{0.53}G_{0.47}aAs$-based absorber layer and excellent efficiency performance, even under short-wavelength (0.85 μm) excitation with a huge absorption process ($\sim$3 μm^{-1}) [15], [16]. This result indicates a much higher defect density and smaller mobility of photo-generated carriers in our GaSb-based material system than that of InP-based ones. The measured defect mapping results of the topmost layer of our wafer structure show a defect density over ten times larger than what is typical of the InP-based PD epitaxy wafers.

Fig. 3(a) and (b) shows the bias-dependent optical-to-electrical (O-E) frequency responses measured under low (0.05 mA) and high (0.3 mA) output photocurrents, respectively. The dotted line in Fig. 3(a) represents the extracted *RC*-limited frequency response of our device, which will be discussed in detail later. As can be seen, under a low output photocurrent (0.05 mA), the widest 3-dB O-E bandwidth is around 6 GHz under −2 V bias and a further increase in the reverse bias voltage (to −4 and −6 V) would lead to a slight degradation in the speed performance. This phenomenon will be discussed later in relation to the measured optical power dependent O-E frequency response, as shown in Fig. 4. On the other hand, when the output photocurrent reaches 0.3 mA, a higher reverse (−4 V) bias voltage is necessary to compensate for the space-charge screening effect induced bandwidth degradation, which is similar to the typical dynamic behavior of high-speed p-i-n PDs [17].

Fig. 4(a) and (b) shows the O-E frequency responses measured under different output photocurrents and two fixed reverse bias voltages −4 and −6 V, respectively. We can clearly see that under a −4 V bias voltage, the O-E bandwidth degrades with the increase in output photocurrent (0.05 to 0.3 mA) as expected, and a high reverse bias (−6 V) can minimize such phenomenon of speed degradation. Under a small output photocurrent (0.05 mA), a high reverse bias (−6 V) degrades the 3-dB O-E bandwidth (5.5–4 GHz). This result can be observed in Fig. 3(a) and can be attributed to the intervalley scattering effect of photo-generated electrons in the $Ga_{0.8}In_{0.2}As_{0.16}Sb_{0.84}$ absorption layer becoming more significant with the increase in reverse bias. This thus leads to a degradation of the internal transit time-limited bandwidth. On the other hand, under a high output photocurrent, the electron/hole induced space-charge screening effect saturates the output of the PD and also diminishes the intervalley scattering effect of the electrons. Similar dynamic behavior has been reported in $InP/In_{0.53}Ga_{0.47}As$-based PDs under short-wavelength (850 nm) excitation. Compared with the case being studied here, the observed O-E bandwidth degradation under high reverse bias voltage is more significant in the $InP/In_{0.53}Ga_{0.47}As$-based PDs due to the fact that a p-type $In_{0.53}Ga_{0.47}As$ absorber has a much larger absorption constant ($\sim$3 versus $\sim$1.5 μm^{-1}) than that of a $Ga_{0.8}In_{0.2}As_{0.16}Sb_{0.84}$ absorption layer under 0.85 and 1.55 μm wavelength excitation, respectively [14]–[16]. A stronger photo-absorption process in the p-type absorber represents a smaller number of photo-generated holes drifting in the intrinsic region and the electrons play a more important role in the dynamic behavior of the PDs.

As shown in Fig. 3(a), the extracted *RC*-limited frequency response can be as high as 13.5 GHz, which implies that the net O-E bandwidth is mainly dominated by the internal carrier transit time. Here, the equivalent circuit modeling technique was performed to extract these parameters for our device [12], [15], [16].

The overall O-E 3-dB bandwidth ($f_{3\mathrm{dB}}$) of a PD is determined by the carrier transport time ($1/f_t$) and the *RC* time constant ($1/f_{RC}$). In order to investigate the internal carrier transport time inside our device, the following equation is adopted [16]:

$$\frac{1}{f_{3\mathrm{dB}}^2} = \frac{1}{f_{RC}^2} + \frac{1}{f_t^2} = (2\pi RC)^2 + \frac{1}{f_t^2} \tag{1}$$

where R is the sum of the parasitic resistance and the load resistance (50 Ω) and C is the total capacitance. Here, the *RC*-limited bandwidth can be extracted by the use of the measured scattering parameters of the microwave reflection coefficients (S_{11}) [12], [15], [16]. Fig. 5(a) shows the adopted equivalent circuit models for the fitting of the S_{11} parameters and the fitted values of each circuit element, except for R_T and C_T, are shown in the table inserted into Fig. 5(b). During the device modeling process for the extraction of the extrinsic f_{RC} for the PD chips, two artificial circuit elements (R_T and C_T) are removed due to the fact that they are

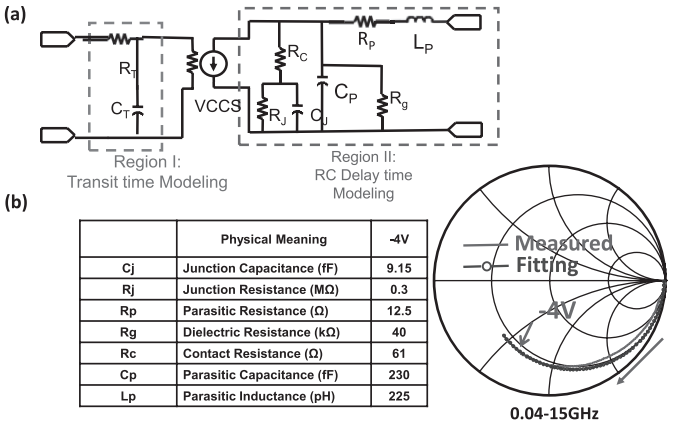

	Physical Meaning	-4V
Cj	Junction Capacitance (fF)	9.15
Rj	Junction Resistance (MΩ)	0.3
Rp	Parasitic Resistance (Ω)	12.5
Rg	Dielectric Resistance (kΩ)	40
Rc	Contact Resistance (Ω)	61
Cp	Parasitic Capacitance (fF)	230
Lp	Parasitic Inductance (pH)	225

Fig. 5. (a) Adopted equivalent circuit model for device modeling. (b) Measured and fitted S_{11} parameters (microwave reflection coefficient) of the device on Smith chart. The arrow head represents the increasing of sweeping frequency. The inserted table shows the values of circuit elements used for the modeling process (voltage-controlled current source).

used to mimic the low-pass frequency response of the internal carrier transit time [12], [15], [16]. Fig. 5(b) shows the fitted and measured S_{11} parameters in the Smith chart while the extracted *RC*-limited frequency responses are given in Figs. 3(a) and 4(a), as discussed above. We can clearly see that the fitted trace matches well with the measured ones from nearly dc to 15 GHz. By use of the extracted *RC*-limited frequency response and (1), the extracted internal carrier transit time-limited bandwidth under 1.55-μm wavelength excitation and 0.05 mA output photocurrent is around 6.7 GHz.

In order to further understand the mechanism behind such a small transit time-limited bandwidth, we simulated the internal frequency responses of our device under 1.55-μm wavelength excitations. The simulation results should let us know the estimated electron/hole drift-velocities and minority diffusion coefficients across intrinsic and p-type $Ga_{0.8}In_{0.2}As_{0.16}Sb_{0.84}$ absorbers, respectively. The adopted drift-diffusion model for bandwidth calculation can be found in [18] and the parameters used for simulation are given in Table II. Here, we assume that our $Ga_{0.8}In_{0.2}As_{0.16}Sb_{0.84}$ absorption layer has a photo-absorption constant as large as 1.5 μm^{-1}, which is close to that of InAs ($\sim$2.0 μm^{-1}) under the same wavelength excitation [19]. These absorption constant values suggest that around 60% of the photo-generated carriers will be concentrated in the topmost 0.6-μm absorption region ($\approx e^{-1}$). The fitted electron/hole drift-velocities and minority (electron) diffusion coefficients in the p-type absorber for the around 7-GHz transit bandwidth are much smaller than the numbers typical in the InP/InGaAs material systems. Take the fitted value of the electron diffusion coefficient ($\sim$200 $cm^2/V \cdot s$) for example. It is over 20 times smaller than that of in the p-type $In_{0.53}Ga_{0.47}As$ absorber ($\sim$5000 $cm^2/V \cdot s$) [17]. This explains the significant recombination process in the p-type absorber and the degradation in the measured EQE value as discussed above.

Fig. 6 represents the photo-generated RF power measured at 6 GHz under three different bias voltages (-3, -4, and -6 V). The ideal relation between the RF power of a 100% modulated large-signal and the average current for

TABLE II
SIMULATION PARAMETERS

	Wavelength:1550 nm
Optical Absorption Constant of $Ga_{0.8}In_{0.2}As_{0.16}Sb_{0.84}$	1.5 μm^{-1}
Effective Absorption Depth (e^{-1})	0.6 μm
Minority Electron Mobility in graded p-doped $Ga_{0.8}In_{0.2}As_{0.16}Sb_{0.84}$	200 cm^2/V-sec
Electron Drift-Velocity in Intrinsic $Ga_{0.8}In_{0.2}As_{0.16}Sb_{0.84}$	2×10^4 m/sec
Hole Drift-Velocity in Intrinsic $Ga_{0.8}In_{0.2}As_{0.16}Sb_{0.84}$	1×10^4 m/sec
Effective Electron Drift Distance at $Ga_{0.8}In_{0.2}As_{0.16}Sb_{0.84}$ Layer	0.5 μm
Effective Hole Drift Distance at $Ga_{0.8}In_{0.2}As_{0.16}Sb_{0.84}$ Layer	0.2 μm

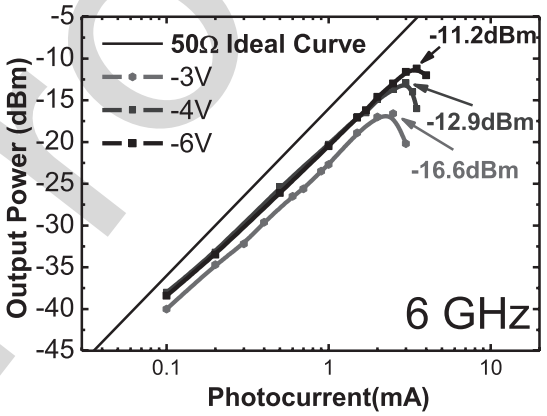

Fig. 6. Measured photo-generated RF power versus photocurrent of demonstrated PD under sinusoidal signal excitations and different reverse biases at an operating frequency of 6 GHz. Solid line: the ideal trace for a 100% modulation depth and 50-Ω load.

a 50 Ω (straight line) load is also plotted for reference. As can be seen, the maximum output saturation current is proportional to the increase in reverse bias voltage. Under -6 V bias, the highest saturation current is limited to around 3.6 mA. In addition, there is an approximately 3–5 dB difference between the measured and ideal RF power under different output photocurrents. Such a discrepancy is mainly due to the high-frequency roll-off in the O-E frequency response of the device itself. As shown in Fig. 3(b), the high-frequency roll-off at 6 GHz in the measured trace under an output photocurrent of 0.3 mA and -6 V reverse bias is around 4 dB, which is consistent with the photo-generated RF power measurement results, as discussed here.

According to our static electric (E) field simulation, the E-field around the p-type absorber and n-type charge layer is around 100 kV/cm under -6 V bias. Use the fitted hole velocities listed in Table II and following (2) [17], the space-charge (hole) induced field under near saturation output ($\sim$3.6 mA) is around $\sim$100 kV/cm. This value is close to the external applied E-field under -6 V bias, which implies that our extracted values for the carrier drift-velocities are

reasonable and consistent with our measurement results. In this equation, E_{sc} represents the space-charge induced field, ε is the dielectric constant of the $Ga_{0.8}In_{0.2}As_{0.16}Sb_{0.84}$ absorption layer, which is around 15 ε_0 [14], and V_c is effective carrier (hole) drift-velocity (1×100^4 m/s). Here, the depletion layer thickness D_{dep} is assumed to be $\sim$0.2 μm. This number is determined by the effective absorption depth (e^{-1}; $\sim$0.6 μm) and the thickness of the p-type absorber ($\sim$0.4 μm) layer in the device structure

$$E_{sc} = J_{max}\left(\frac{D_{dep}}{\varepsilon V_c}\right). \quad (2)$$

The results indicate that the saturation power in our device is limited by the small carrier drift-velocity and its induced space-charge screening effect.

IV. Conclusion

A high-speed and high-power GaSb-based PD with a cutoff wavelength at around 2.5 μm was demonstrated for the first time. The addition of a partially depleted absorber layer has been implemented in our structure to minimize the space-charge screening effect and improve the high-power/speed performance. Furthermore, a miniaturized device size (active diameter: 8 μm) is adopted to enlarge the *RC*-limited bandwidth. With careful passivation to minimize the influence of the surface state, low dark current can still be sustained ($\sim$0.7 μA at -2 V) in such a small device. According to the measurement and modeling results under 1.55-μm optical wavelength excitation, the slow carrier drift/diffusion time inside our $Ga_{0.8}In_{0.2}As_{0.16}Sb_{0.84}$ active layers is the major factor limiting the speed and output power. A 3.6-mA saturation current measured at the 6-GHz operating frequency can be achieved. The PD demonstrates good speed and power performance at a wavelength of 2.5 μm so should find applications in midinfrared (2–5 μm) Si photonics, high-resolution/frame rate LIDAR image sensors, and photo-receivers in next-generation optical fiber communication channels.

References

[1] R. Soref, "Mid-infrared photonics in silicon and germanium," *Nature Photon.*, vol. 4, pp. 495–497, Aug. 2010.

[2] A. Joshi and S. Datta, "High-speed, large-area, p-i-n InGaAs photodiode linear array at 2-micron wavelength," *Proc. SPIE*, vol. 8353, p. 83533D, May 2012.

[3] J. E. Bowers, A. K. Srivastava, C. A. Burrus, M. A. DeWinter, M. A. Pollack, and J. L. Zyskind, "High-speed GaInAsSb/GaSb PIN photodetectors for wavelengths to 2.3 μm," *Electron. Lett.*, vol. 22, pp. 137–138, Jan. 1986.

[4] N. Ye *et al.*, "InGaAs surface normal photodiode for 2 μm optical communication systems," *IEEE Photon. Technol. Lett.*, vol. 27, no. 14, pp. 1469–1472, Jul. 15, 2015.

[5] Y. Miyamoto, M. Yoneyama, K. Hagimoto, T. Ishibashi, and N. Shimizu, "40 Gbit/s high sensitivity optical receiver with uni-travelling-carrier photodiode acting as decision IC driver," *Electron. Lett.*, vol. 34, no. 2, pp. 214–215, Jan. 1998.

[6] X. Li *et al.*, "High-saturation-current InP-InGaAs photodiode with partially depleted absorber," *IEEE Photon. Technol. Lett.*, vol. 15, no. 9, pp. 1276–1278, Sep. 2003.

[7] Y. Muramoto and T. Ishibashi, "InP/InGaAs pin photodiode structure maximising bandwidth and efficiency," *Electron. Lett.*, vol. 39, no. 24, pp. 1749–1750, Nov. 2003.

[8] I. A. Andreev *et al.*, "High-speed photodiodes for the mid-infrared spectral region 1.2–2.4 μm based on GaSb/GaInAsSb/GaAlAsSb heterostructures with a transmission band of 2–5 GHz," *Semiconductors*, vol. 47, no. 8, pp. 1103–1109, Aug., 2013.

[9] A. Rakovska *et al.*, "Room temperature InAsSb photovoltaic midinfrared detector," *Appl. Phys. Lett.*, vol. 77, no. 3, pp. 397–399, Jul. 2000.

[10] X. Li *et al.*, "A partially depleted absorber photodiode with graded doping injection regions," *IEEE Photon. Technol. Lett.*, vol. 16, no. 10, pp. 2326–2328, Oct. 2004.

[11] Y.-S. Wu *et al.*, "High-performance evanescently edge coupled photodiodes with partially p-doped photoabsorption layer at 1.55-μm wavelength," *IEEE Photon. Technol. Lett*, vol. 17, no. 4, pp. 878–880, Apr. 2005.

[12] J.-M. Wun *et al.*, "Photonic high-power continuous wave THz-wave generation by using flip-chip packaged uni-traveling carrier photodiodes and a femtosecond optical pulse generator," *J. Lightw. Technol.*, vol. 34, no. 4, pp. 1387–1397, Feb. 15, 2016.

[13] T. I. Voronina *et al.*, "The effect of tellurium diffusion from an *n*-GaSb:Te substrate on the properties of GaInAsSb solid solutions grown from lead-containing melt," *Semiconductors*, vol. 39, pp. 308–312, Mar. 2005.

[14] M. P. Mikhailova, *Handbook Series on Semiconductor Parameters*, vol. 2, M. Levinshtein, S. Rumyantsev, and M. Shur, Eds. London, U.K.: World Scientific, 1999, pp. 180–205.

[15] J.-W. Shi, C.-Y. Li, K.-L. Chi, J.-M. Wun, Y.-M. Hsin, and S. D. Benjamin, "Large-area p-i-n photodiode with high-speed and high-efficiency across a wide optical operation window (0.85 to 1.55 μm)," *IEEE J. Sel. Topics Quantum Electron.*, vol. 20, no. 6, Nov./Dec. 2014, Art. no. 3800807.

[16] J.-W. Shi, K.-L. Chi, C.-Y. Li, and J.-M. Wun, " Dynamic analysis of high-efficiency InP-based photodiode for 40 Gbit/s optical interconnect across a wide optical window (0.85 to 1.55 μm)," *J. Lightw. Technol.*, vol. 33, no. 4, pp. 921–927, Feb. 15, 2015.

[17] K. Kato, "Ultrawide-band/high-frequency photodetectors," *IEEE Trans. Microw. Theory Techn.*, vol. 47, no. 7, pp. 1265–1281, Jul. 1999.

[18] J.-W. Shi, Y.-H. Liu, and C.-W. Liu, "Design and analysis of separate-absorption-transport-charge-multiplication traveling-wave avalanche photodetectors," *J. Lightw. Technol.*, vol. 22, no. 6, pp. 1583–1590, Jun. 2004.

[19] M. P. Mikhailova, *Handbook Series on Semiconductor Parameters*, vol. 1, M. Levinshtein, S. Rumyantsev, and M. Shur, Eds. London, U.K.: World Scientific, 1996, pp. 147–168.

Jhih-Min Wun was born in Taoyuan, Taiwan, in 1988. He is currently pursuing the Ph.D. degree with the Department of Electrical Engineering, National Central University, Taoyuan.

His current research interests include high-speed optoelectronic device measurement and sub-THz high-speed photodiode.

Yu-Wen Wang was born in Kaohsiung, Taiwan, in 1992. He is currently pursuing the master's degree with the Department of Electrical Engineering, National Central University, Taoyuan, Taiwan.

His current research interests include high-speed and high-power photodiode.

Yi-Han Chen was born in Kaohsiung, Taiwan, in 1992. He is currently pursuing the master's degree with the Department of Electrical Engineering, National Central University, Taoyuan, Taiwan.

His current research interests include high-speed and high-sensitivity avalanche photodiode.

John E. Bowers (F'93) holds the Fred Kavli Chair in Nanotechnology, and is the Director of the Institute for Energy Efficiency and a Professor with the Department of Materials and Electrical and Computer Engineering, University of California at Santa Barbara, Santa Barbara, CA, USA. He is a Co-Founder of Aurrion, Santa Barbara, CA, Aerius Photonics, Ventura, CA, USA, and Calient Networks, Goleta, CA, USA.

Jin-Wei Shi (M'03–SM'12) was born in Kaohsiung, Taiwan in 1976.

He joined the Department of Electrical Engineering, National Central University, Taoyuan, Taiwan, in 2003, where he has been a professor since 2011. He joined the Department of Materials and Electrical and Computer Engineering, University of California at Santa Barbara, Santa Barbara, CA, USA, as a Visiting Professor, in 2011 and 2012 and 2016. He has authored or co-authored over four book chapters, 120 journal papers, 180 conference papers, and hold 30 patents. His current research interests include ultra-high speed/power photodetectors, electro-absorption modulator, THz photonic transmitter, and VCSELs.

Dr. Shi was a recipient of 2010 Da-You Wu Memorial Award.